AIAA 81-4202

Coherent Structures Induced by Two Simultaneous Sparks in an Axisymmetric Jet

M. Sokolov,* S. J. Kleis,† and A.K.M.F. Hussain‡
University of Houston, Houston, Texas

The axisymmetric mixing layer of a 12.7-cm-diam circular air jet at the exit speed of 20 m/s has been excited by two sparks fired simultaneously at diametrically opposite points near the lip. The resulting large-scale coherent structure—buried in the large-amplitude turbulent fluctuations in the mixing layer—has been educed at three streamwise stations and along three azimuthal planes. Spatial distributions of the coherent structure velocity perturbations, coherent Reynolds stress, vorticity, pseudo-streamfunctions, intermittency, as well as phase averages of the background fluctuation intensities and Reynolds stress have been deduced. The coherent Reynolds stress is considerably larger than the background turbulence Reynolds stress and the coherent peak vorticity is noticeably larger than time-mean peak vorticity. The coherent structure becomes progressively weaker with increasing x. The azimuthal variations of the educed contours suggest that the induced structure is a naturally occurring structure triggered by the sparks and is essentially axisymmetric; it undergoes a rapid change in its geometry, dynamics, and convection velocity as it travels downstream.

Introduction

As a part of our continuing effort to understand the nature and the role of the large-scale coherent structure (which are presumed to be of major significance in turbulent shear flows[1-8]) our earlier time-averaged measurements in the axisymmetric mixing layer have been extended to investigations of the structures based on hot-wire measurements and flow visualization studies. These included investigations involving axisymmetric excitation as well as no-excitation cases. Flow visualization of a high Reynolds number, unexcited, axisymmetric mixing layer by Hussain and Clark[8] has shown that the nature of the structures and their interactions are indeed complex. The large dispersion of the shape, size, orientation, strength, "age," and convection velocity of naturally occurring structures made eduction of these structures prohibitive. Studies of coherent structures induced by controlled disturbances, including the present one, offer a considerable simplification in the eduction of structure properties because of availability of the structure phase from the induced excitation. Note that there is an inherent difference between coherent structures induced by impulsive and sinusoidal disturbances. In the former case, the induced structures are separated by natural structures; consequently, the structure interactions are likely to be different from the latter case where all structures are induced.

In an attempt to study the response of an axisymmetric mixing layer to a localized disturbance, a spark was produced between two needles in the nozzle boundary layer of an air jet. The spark-induced large-scale structure in the shear layer is called a "spot" for lack of a better name. The details of experimental and digital analysis techniques, the flow initial condition, and the basic flow characteristics of the axisymmetric mixing layer without the spot were explained by Sokolov et al.[9] The analytical considerations in the study of the coherent structure dynamics in general, and the spatial details of the spot-induced velocity field, coherent Reynolds stress, vorticity, streamlines, pseudo-streamfunctions, intermittency, and background turbulence intensities and Reynolds stress, as well as the spot dynamics including interaction between coherent and phase-random fields, have been discussed by Hussain et al.[10]

References 9 and 10 covered data in one plane (bisecting the needles) and they left unanswered questions regarding the azimuthal variation of "spot" structure, the mechanism of formation of the spot, and the nature of its interactions with other naturally occurring structures. In an attempt to obtain these answers, it was decided to induce structures with two concurrent sparks and investigate the evolutions and interactions of these structures. It was felt that two sparks located at diametrically opposite points and fired simultaneously would either trigger structures which would interact in an interesting manner or the two sparks would simultaneously induce a combined structure in the mixing layer different from the single spark-induced spot. It was expected that the measurements, apart from being an inherently interesting study on its own, would further our understanding of the evolution of large-scale coherent structures, their mutual interactions, and their interactions with the background turbulence in the near field of an axisymmetric jet. The control of the near field coherent structure of a jet may also find application in the control of mixing and jet noise production.

Procedures

The spark-induced coherent structure was studied in the near field of an air jet 12.7 cm in diameter D, discharging into a large laboratory with controlled temperature, humidity, and traffic. The facility consists of a number of modules connected together through flexible couplings. The 2.8 m long settling chamber 76 cm in diameter contains a number of screens. The flow emerges into the laboratory through an axisymmetric nozzle with a contraction ratio of 36:1, terminated by a tip with a wedge angle of 20 deg. The jet is driven by a blower with a dc motor whose speed can be held constant over long runs. Further details of the facility have been given elsewhere.[11]

The study has been carried out for the exit speed U_e of 20 m/s with the longitudinal fluctuation intensity of 0.3% at the exit plane centerline. The sparks are generated between two needle tips in the middle of Bakelite inserts so that the needles are insulated from each other. The needle tips (0.085 cm diam) were mounted nearly flush with the hydraulically smooth wall 6.8 cm upstream from the nozzle exit. The sparks were generated between the two needles 1.4 cm apart by an ordinary ignition coil; the needles were located along an azimuthal line so that the line spark was aligned azimuthally.

Received July 29, 1980; revision received March 13, 1981.

*Presently, College of Engineering, Tel-Aviv University, Israel.
†Assistant Professor, Dept. of Mechanical Engineering. Member AIAA.
‡Professor, Dept. of Mechanical Engineering. Associate Fellow AIAA.

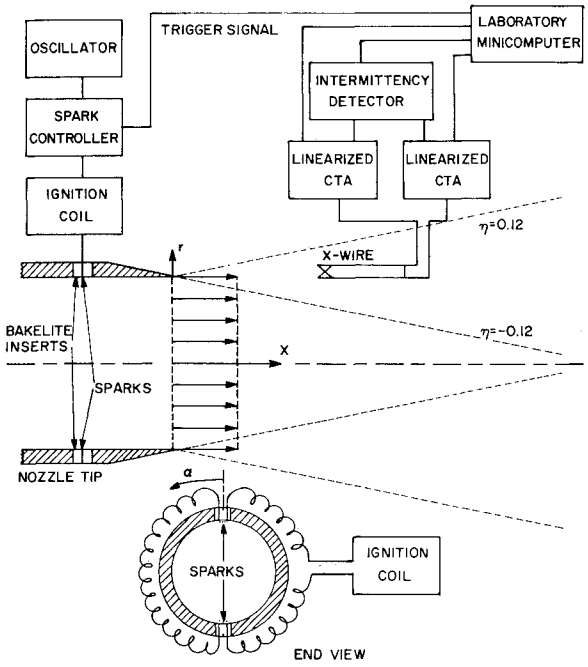

Fig. 1 Schematic of spark arrangement, measurement technique, and coordinates.

The sparks were triggered by a function generator which provided the phase reference between the spark trigger and initiation of on-line computer-controlled data acquisition. To insure identical timing of the two sparks, they were connected in series. Care was taken to make the two sets of needles and their spacing as equal as possible so that the two disturbances would be identical. Figure 1 shows the schematic of the spark generation and data acquisition arrangements and the coordinate system.

In consideration of the prohibitively long computer time required for signal alignment, it was necessary to limit data acquisition to a few x stations. As a result, x-wire measurements were made at three stations, namely $x/D=1.5$, 3.0, and 4.5, where D is the jet exit diameter. For symmetry considerations, it was decided that the two sparks should be fired at diametrically opposite points in the nozzle exit and, again for symmetry, that data would be required in only one quadrant (say $0\leq\alpha\leq 90$ deg); $\alpha=0$ deg denotes the plane of symmetry through one set of needles, i.e., the plane bisecting one of the sparks (see Fig. 1). Data were recorded in three azimuthal planes passing through the jet axis, corresponding to the values of the azimuthal angle α of 0, 45, and 90 deg. At each location, 200 realizations of instantaneous signals [of $u(t)$, $v(t)$, and intermittency signal $I(t)$] were recorded in such a way that the realization captured the spot "footprint." For details of the intermittency detection circuit, see Refs. 10 and 12. The spot signature was captured by phase locking to the spark trigger the on-line signal digitization (at 8.4 kHz for each channel) by the laboratory computer (HP2100S). At each station in the $\alpha=0$ deg plane, data were recorded at eight radial positions corresponding to the values of $\eta[\equiv(r-D/2)/x]=0.12, 0.09, 0.06, 0.03, 0, -0.03, -0.06$, and the jet centerline. In the $\alpha=45$ and 90 deg planes, data were recorded at fewer transverse locations, i.e., at five radial positions corresponding to $\eta=0.12$, 0.06, 0, -0.06, and the jet centerline. Since the virtual origin of the shear layer is near the lip (i.e., $x_0=-0.13D$), an $\eta=$ const line essentially represents a $U/U_e=$ const line. For correspondence between $\eta=$ const lines to the $U/U_e=$ const lines, see Ref. 9. Thus, consistent with Bruun[4] and Yule,[5] the radial coordinate is denoted by η. The exit mean velocity profile agrees with the Blasius profile with the shape factor of 2.59. The congruence of non-dimensionalized mean velocity and fluctuation intensity profiles, the linear evolution of the mixing layer thickness, and full development of the spectra indicate that the mixing layer has essentially achieved self-preservation for $x/D\geq 0.75$; for further details, see Ref. 11.

The data analysis procedure, explained in Ref. 9, will be briefly recapitulated here. At each x and η, three simultaneous signals $u(t)$, $v(t)$, and $I(t)$ were digitized on-line each at the rate of 8.4k words/s and recorded on digital magnetic tape for later processing. For any signal, say $u(t)$, $v(t)$, or $I(t)$, a straightforward phase average of 200 realizations at each location gives the zero iteration ensemble average. Each realization was then time shifted with respect to this average in order to maximize its cross correlation with the average. A phase average of these shifted realizations gave the first iteration ensemble average. The procedure was continued until convergence was reached. In order to enhance the coherent structure signature, realizations requiring excessive time shifts (i.e., larger than three times the standard deviation σ_t of the time shifts at each η and x) were discarded. Also, each realization was low-pass filtered at 500 Hz in order to accelerate the iteration process for maximization of cross correlation. Note that time shifts for optimum alignment were determined for $u(t)$ signals only; for consistency, $v(t)$ and $I(t)$ signals were given identical time shifts as the $u(t)$ signal at each location. Histograms of the time shifts as well as the radial distribution of the fraction of realizations rejected for the single spark were discussed in Ref. 9.

Results and Discussion

In order to interpret the data it is necessary to recognize that in the presence of the spot, the instantaneous flow variables consist of coherent and random contributions. That is,

$$u=u_p+u_r, \quad v=v_p+v_r \tag{1}$$

so that u_pv_p and $\langle u_rv_r\rangle$ are, respectively, the coherent and background turbulence Reynolds stresses and $\zeta_p=\partial v_p/\partial x-\partial u_p/\partial r$ the coherent vorticity. However, considering the flowfield as the combination of the coherent structures and turbulence superimposed on the mean field, one can use the classical decomposition,[13]

$$u=U+\tilde{u}_p+u_r, \quad v=V+\tilde{v}_p+v_r \tag{2}$$

Then, $\tilde{u}_p\tilde{v}_p$ will be the coherent Reynolds stress. Furthermore, the intensity f_r' of the background fluctuation f_r at any phase ϕ is defined as

$$f_r'=\left[\lim_{N\to\infty}\frac{1}{N}\sum_{n=1}^{N}f_r^2(\phi+n2\pi)\right]^{1/2} \tag{3}$$

As explained in Ref. 10, integration of the $u_p(x,t)$ data in r provides spatial distributions of the *pseudo-streamfunction* $\langle\psi\rangle$. It was shown in Ref. 10 that values of $\langle\psi\rangle$ when plotted as contours are quite helpful in understanding the dynamics of the coherent structures and deducing their convection velocities. Contours of constant values of $\langle\psi\rangle$ are shown in Figs. 2-4 for $x/D=1.5$, 3.0, and 4.5, respectively. In each of these figures, cases a, b, and c represent the azimuthal planes for α values of 0, 45, and 90 deg, respectively.

The $\langle\psi\rangle$ contours have been plotted with respect to a frame convected downstream with the velocity $U_c=0.66\,U_e$. That is

$$\langle\psi\rangle(r,T)=\int_0^r r'(u_p-U_c)\,dr'$$

The time T (in milliseconds) with respect to the spark trigger is shown as the abscissa; the values of the nondimensional time U_eT/x corresponding to $T=40$ ms are 4.4, 2.2, and 1.46 at $x/D=1.5$, 3.0, and 4.5, respectively.

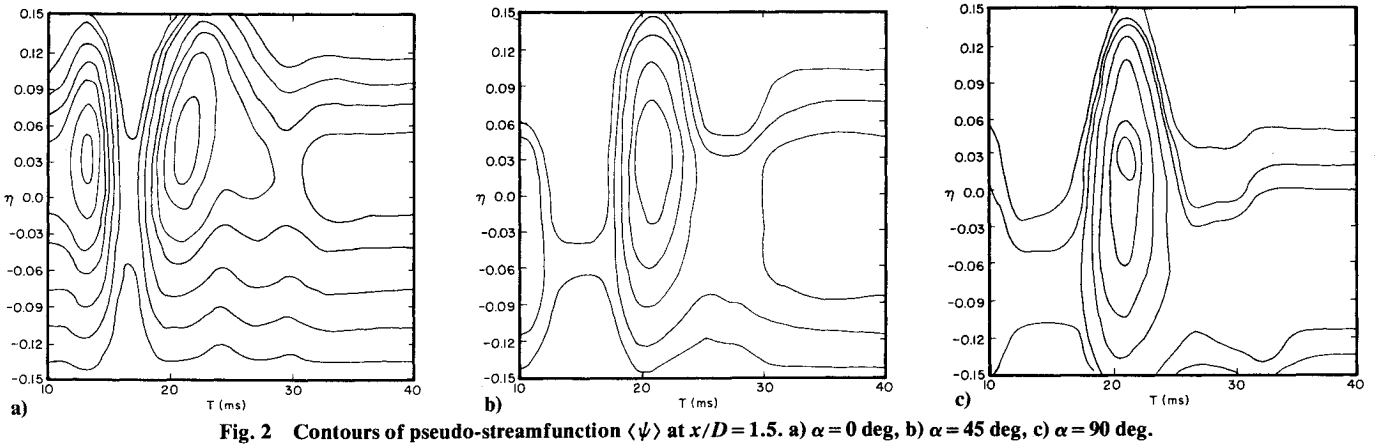

Fig. 2 Contours of pseudo-streamfunction $\langle\psi\rangle$ at $x/D=1.5$. a) $\alpha=0$ deg, b) $\alpha=45$ deg, c) $\alpha=90$ deg.

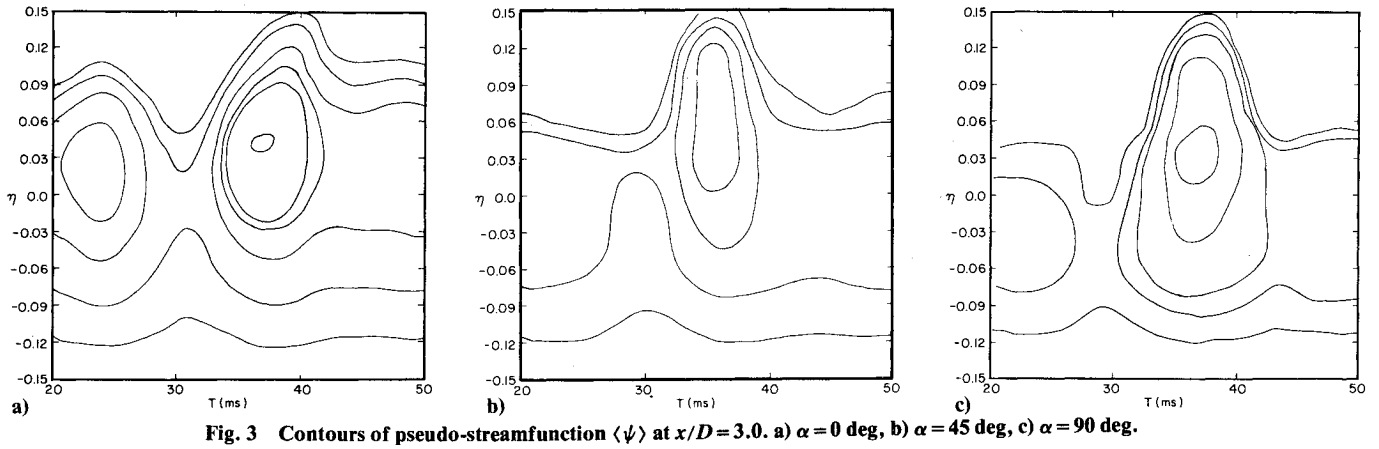

Fig. 3 Contours of pseudo-streamfunction $\langle\psi\rangle$ at $x/D=3.0$. a) $\alpha=0$ deg, b) $\alpha=45$ deg, c) $\alpha=90$ deg.

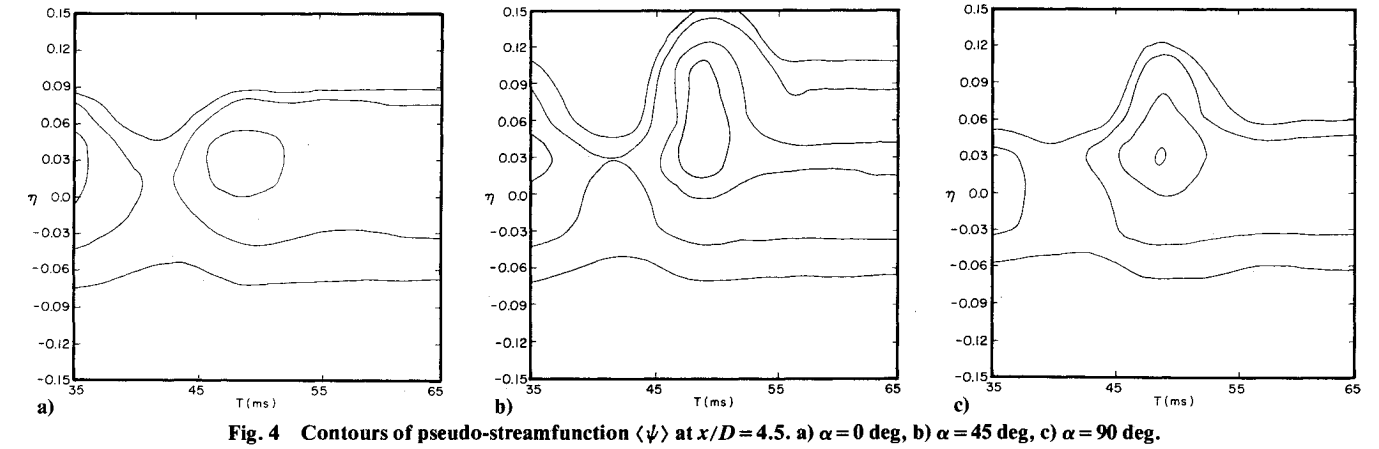

Fig. 4 Contours of pseudo-streamfunction $\langle\psi\rangle$ at $x/D=4.5$. a) $\alpha=0$ deg, b) $\alpha=45$ deg, c) $\alpha=90$ deg.

Consider first the structure in the $\alpha=0$ deg plane. The structure is centered at about $T=21$, 37, and 49 ms at $x/D=1.5$, 3.0, and 4.5, respectively. Between the three stations, the structure changes noticeably. At $x/D=1.5$, the front of the structure (i.e., at lower T) is characterized by intense shear, while the trailing end is more diffuse. At $x/D=4.5$, the structure is more diffuse all around. Note that this picture is somewhat distorted by the fact that in the (η, T) plane, the lateral distances are compressed with increasing x. These figures suggest that the spot lateral extent increases with x but this increase is not as fast as that of the thickness of the shear layer. This is to be expected since the linear increase of the mixing-layer width with x will be contributed by the increased lateral wandering of the structure rather than by a corresponding increase in the size of the structure alone. The progressive increase in x of the ΔT range of the spot is an indication of the average streamwise growth of the spot.

The apparent difference in the structure in front (i.e., at smaller T) of the spot between 0 deg and the other angles is an artifact of the alignment procedure. A careful consideration of the velocity time series of 45 and 90 deg indicates a larger variation in spacing of u_p local maxima. The alignment procedure shifts the time series to the largest peak of the zero iteration ensemble average. As a result, the other local maximum (see Ref. 9, Fig. 17) is reduced in amplitude in the final ensemble average of Figs. 2-4. This effect is less pronounced at 0 deg, possibly due to a larger disturbance amplitude. The smaller structure following the spot (i.e., at larger T) in Figs. 2 may indicate the remnant of the decaying boundary-layer spot following the mixing-layer spot. It is

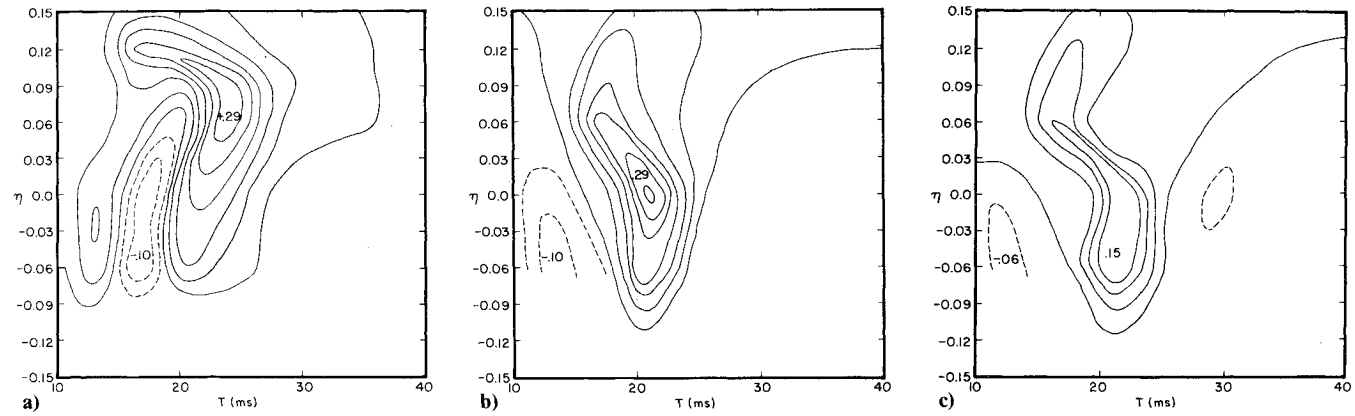

Fig. 5 Contours of $\tilde{u}_p/U_e$ at $x/D=1.5$. a) $\alpha=0$ deg, b) $\alpha=45$ deg, c) $\alpha=90$ deg.

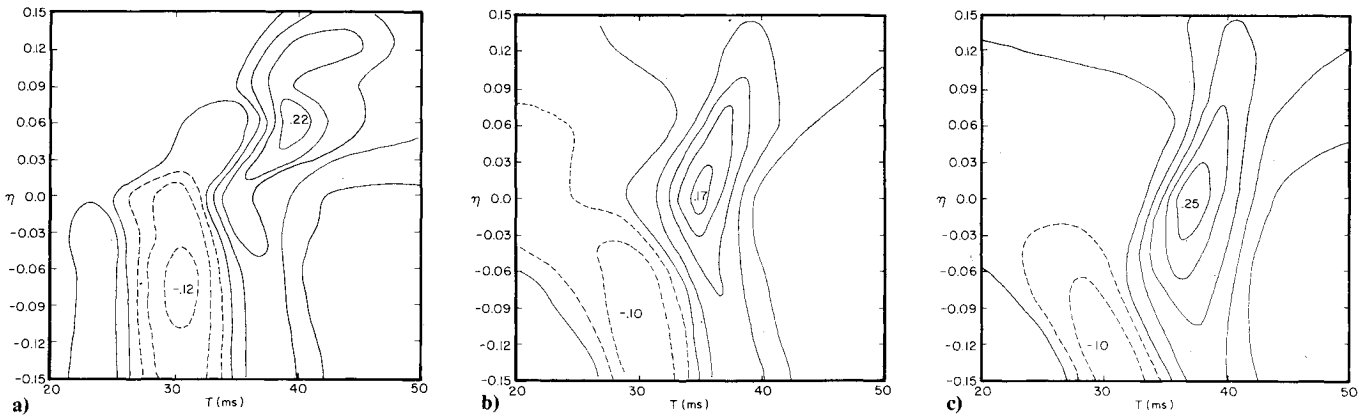

Fig. 6 Contours of $\tilde{u}_p/U_e$ at $x/D=3.0$. a) $\alpha=0$ deg, b) $\alpha=45$ deg, c) $\alpha=90$ deg.

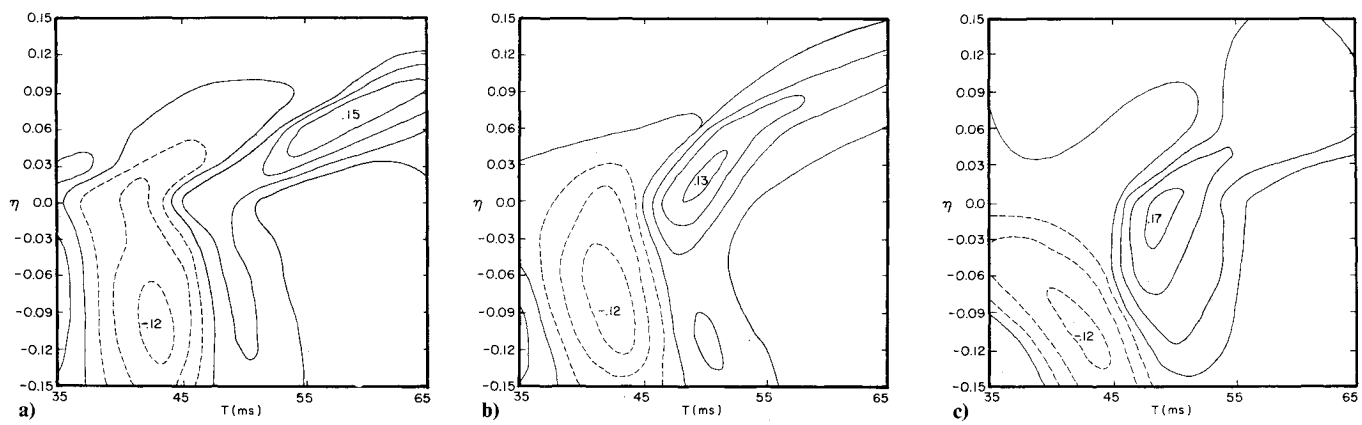

Fig. 7 Contours of $\tilde{u}_p/U_e$ at $x/D=4.5$. a) $\alpha=0$ deg, b) $\alpha=45$ deg, c) $\alpha=90$ deg.

likely that the spot would be embedded in the naturally occurring structures, but these random structures should leave no footprint in the aligned ensemble average data.

Comparison of the $\langle\psi\rangle$ contours for the two-spark and single-spark cases in the $\alpha=0$ deg plane (i.e., comparing Figs. 2a, 3a, and 4a with Figs. 11a-c of Ref. 10) show that the pseudo-streamfunctions are quite similar.

Considering the data at different α, some differences between the $\langle\psi\rangle$ contours are discernible. However, these differences are not large; especially, the locations (in T) of the peak values of $\langle\psi\rangle$ are essentially the same. Note that for $x/D=1.5$, the radial extent of the spot is largest for $\alpha=90$ deg, i.e., in a plane normal to that of the two sparks, and smallest for $\alpha=0$ deg. These variations persist at $x/D=3.0$ but are least at $x/D=4.5$. The explanation for this azimuthal dependence is not known. However, a part of the observed differences is attributable to the limited data at $\alpha=45$ and 90 deg.

Contours of the coherent structure streamwise velocity $\tilde{u}_p$ are shown in Figs. 5-7 for $x/D=1.5$, 3.0, and 4.5, respectively. In each, cases a, b, and c represent data for $\alpha=0$, 45, and 90 deg, respectively. The positive values are denoted by solid lines and negative values by dotted lines. Comparing the $\tilde{u}_p$ contours for single-spark and double-spark cases for $\alpha=0$ deg (i.e., comparing Figs. 5a, 6a, and 7a with Figs. 17a-c of Ref. 9), there is excellent agreement on the high-speed side of the contours as well as on the locations of peak $\tilde{u}_p$. However, the low-speed side is somewhat different; note that at $x/D=1.5$, the locations of the peak values of $\tilde{u}_p$ at $\alpha=0$, 45, and 90 deg agree but not the detailed structure, and the contours at $\alpha=0$ and 90 deg are noticeably different from each other. With increasing x, the variations between $\tilde{u}_p$ contours at different α progressively disappear; note the close agreement between the peak values of negative peaks for different α at $x/D=4.5$. The region of negative $\tilde{u}_p$, in front of the structure (i.e., at lower T) toward the high-speed side,

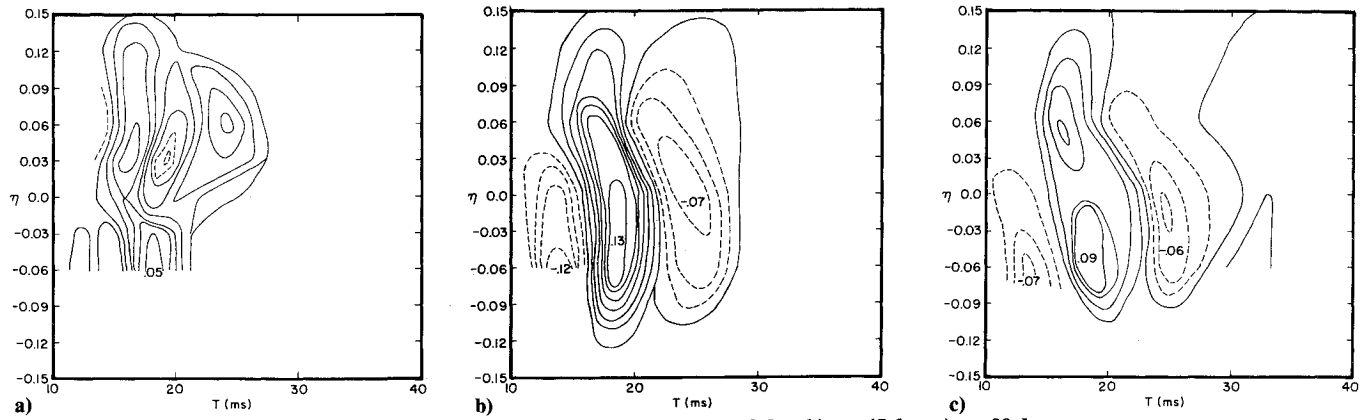

Fig. 8 Contours of $\tilde{v}_p/U_e$ at $x/D=1.5$. a) $\alpha=0$ deg, b) $\alpha=45$ deg, c) $\alpha=90$ deg.

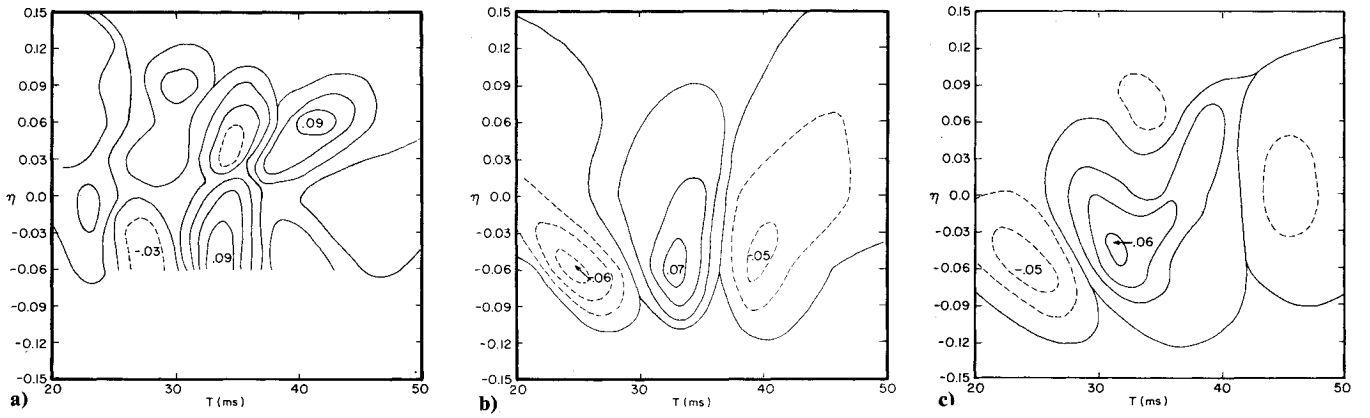

Fig. 9 Contours of $\tilde{v}_p/U_e$ at $x/D=3.0$. a) $\alpha=0$ deg, b) $\alpha=45$ deg, c) $\alpha=90$ deg.

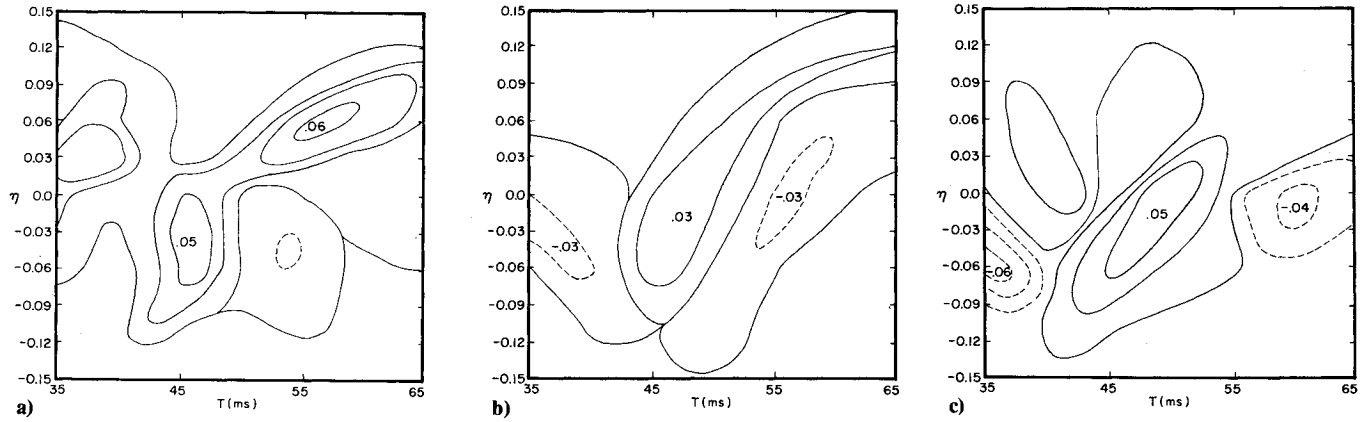

Fig. 10 Contours of $\tilde{v}_p/U_e$ at $x/D=4.5$. a) $\alpha=0$ deg, b) $\alpha=45$ deg, c) $\alpha=90$ deg.

suggests a slowing down of the flow, somewhat similar to the stagnation region in front of a rotating cylinder. Note that with increasing x, the extent of the negative $\tilde{u}_p$ region increases and the streamwise separation between the positive and negative peaks increases, consistent with the increase of the spot length with x.

The distributions of the radial velocity $\tilde{v}_p$ for $x/D=1.5$, 3.0, and 4.5 are shown in Figs. 8-10, respectively. Note that for $x/D=1.5$, the $\tilde{v}_p$ contours at $\alpha=45$ and 90 deg are quite similar, while both are quite different from those at $\alpha=0$ deg. The clear differences between $\tilde{v}_p$ contours at different α, especially at $x/D=3.0$ and 4.5, suggest that $\tilde{v}_p$ is not a clear indicator of the coherent structure boundaries. Comparison of the $\tilde{u}_p$ and $\tilde{v}_p$ contours show that they are quite different.

If $\tilde{u}_p\tilde{v}_p$ is regarded as the organized momentum transport, then it is clear that it will be large only when the peaks of the $\tilde{u}_p$ and $\tilde{v}_p$ contours agree. Comparison of the contours of $\tilde{u}_p\tilde{v}_p$ (not presented) with the $\tilde{u}_p$ and $\tilde{v}_p$ contours show that the $\tilde{u}_p\tilde{v}_p$ contours are primarily influenced by $\tilde{v}_p$ contours, an observation made in Refs. 10 and 14.

Since the coherent structure is not riding on top of the time-mean flow, the latter being essentially due to superposition of many structures, $\tilde{u}_p\tilde{v}_p$ is not the coherent structure Reynolds stress. Since on an instantaneous basis, the phase-averaged velocity field (u_p, v_p) is essentially due to the coherent structure, the coherent Reynolds stress $(uv)_c$ should be $(u_p - U_c)v_p$ in a frame advected with the structure as a whole, where U_c is the structure convection velocity. Figures 11-13

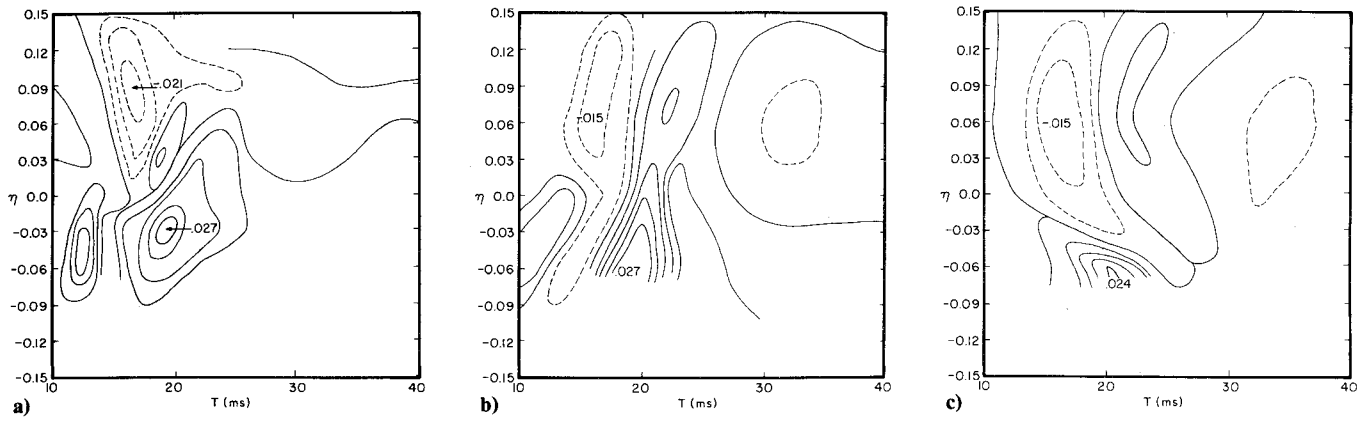

Fig. 11 Contours of $(uv)_c/U_e^2$ at $x/D=1.5$. a) $\alpha=0$ deg, b) $\alpha=45$ deg, c) $\alpha=90$ deg.

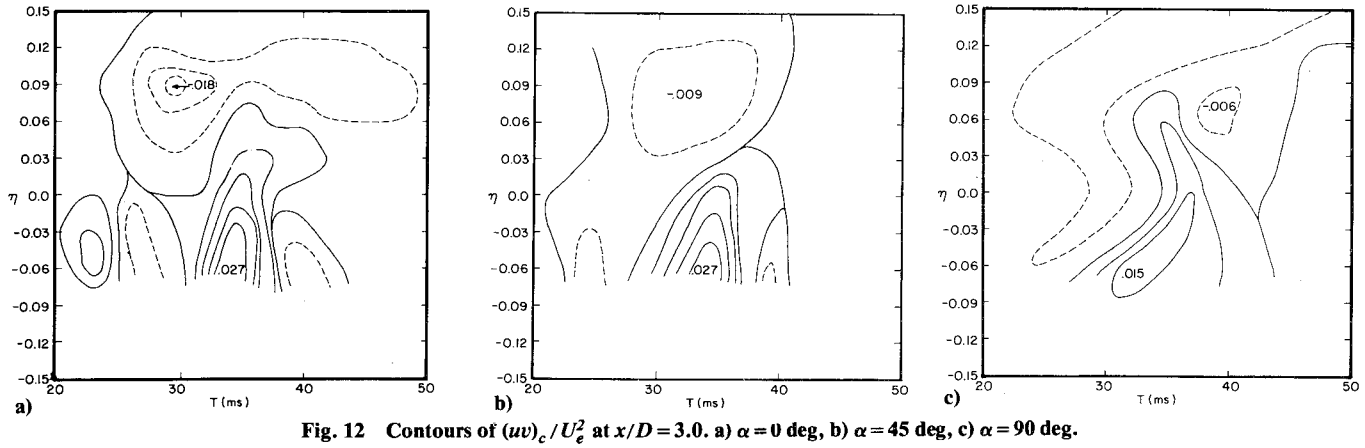

Fig. 12 Contours of $(uv)_c/U_e^2$ at $x/D=3.0$. a) $\alpha=0$ deg, b) $\alpha=45$ deg, c) $\alpha=90$ deg.

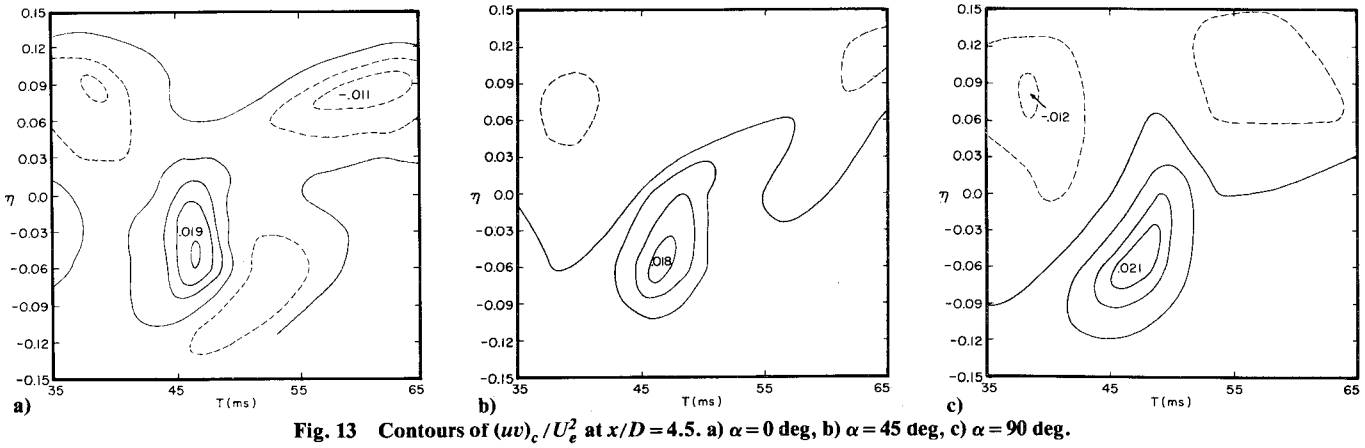

Fig. 13 Contours of $(uv)_c/U_e^2$ at $x/D=4.5$. a) $\alpha=0$ deg, b) $\alpha=45$ deg, c) $\alpha=90$ deg.

show the contours of coherent Reynolds stress $(uv)_c$ contours for $x/D=1.5$, 3.0 and 4.5, respectively. The noticeable differences between $(uv)_c$ contours at different α can be partly attributed to limited η locations at which data have been obtained and to limited size of the realizations.

However, in the laboratory frame the total transport is $u_p v_p$, which also includes transports such as $\tilde{u}_p \bar{V}$ and $\bar{U}\tilde{v}_p$ in addition to $\tilde{u}_p \tilde{v}_p$. For comparison, the contours of $u_p v_p$ for the $\alpha=0$ deg plane only are shown in Figs. 14a-c for $x/D=1.5$, 3.0, and 4.5, respectively. Note the similarity between these three contours.

Considering the spot to be a large-scale vortical structure spanning the width of the mixing layer, the momentum transport should be positive at the front on the high-speed side and at the back on the low-speed side, a picture revealed well by Fig. 14a. The structure center in this figure should be midway between the positive and negative contours, say at $T=53$ ms. Comparison of Figs. 13a and 14c (which represent $(uv)_c$ and $u_p v_p$, respectively, for the same station) highlights the differences between the spot transport viewed from the structure or laboratory frames. The negative transport region in Fig. 13a (with respect to a reference frame convected with the structure velocity) becomes positive in the laboratory frame because the low-speed region moves downstream in the laboratory frame while it is upstream in the structure center frame. In spite of the apparent similarity between the contours in Figs. 13a and 14c, the values are quite different because of the different reference frames used. Note the increasing time separation between the two peak contours between Figs. 14a-c, suggesting progressive streamwise enlargement and tilt [i.e., clockwise rotation in the (η, T) plane] of the spot with increasing x. Since a constant value of η represents larger r with increasing x, it is clear the spot transverse extent also increases with x.

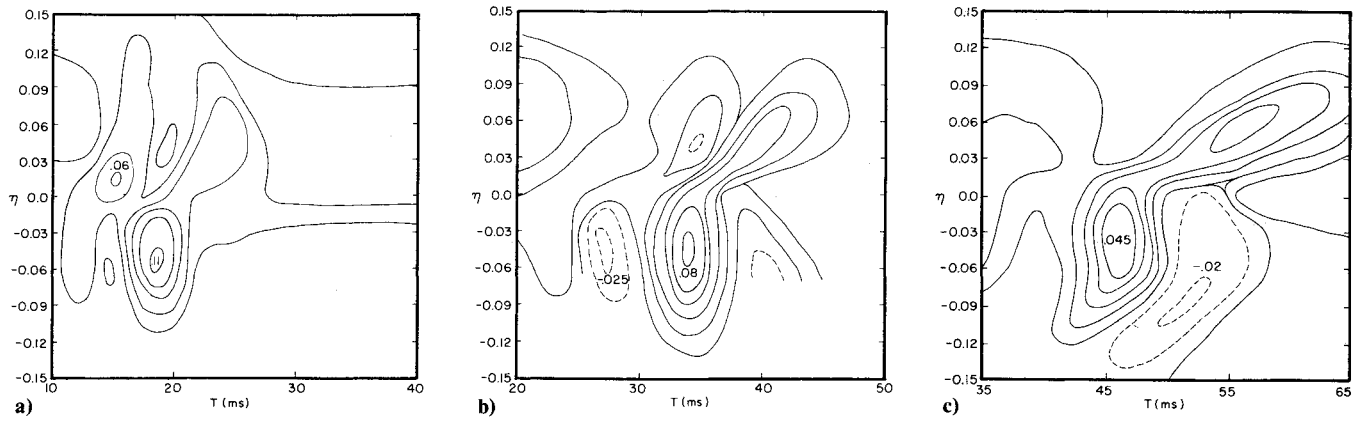

Fig. 14 Coherent Reynolds stress $u_p v_p / U_e^2$ for $\alpha = 0$ deg. a) $x/D = 1.5$, b) $x/D = 3.0$, c) $x/D = 4.5$.

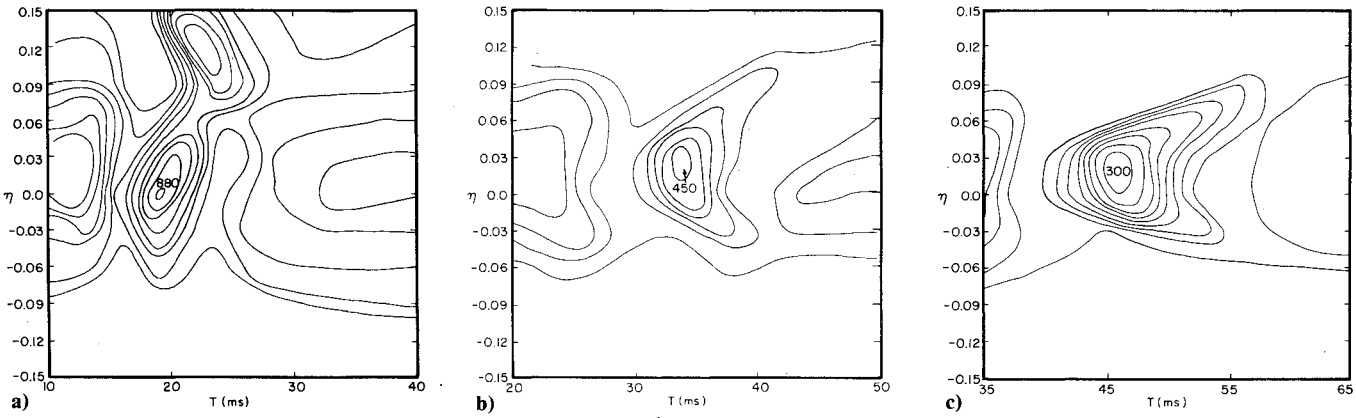

Fig. 15 Contours of coherent vorticity ζ_p (in s^{-1}) for $\alpha = 0$ deg. a) $x/D = 1.5$, b) $x/D = 3.0$, c) $x/D = 4.5$.

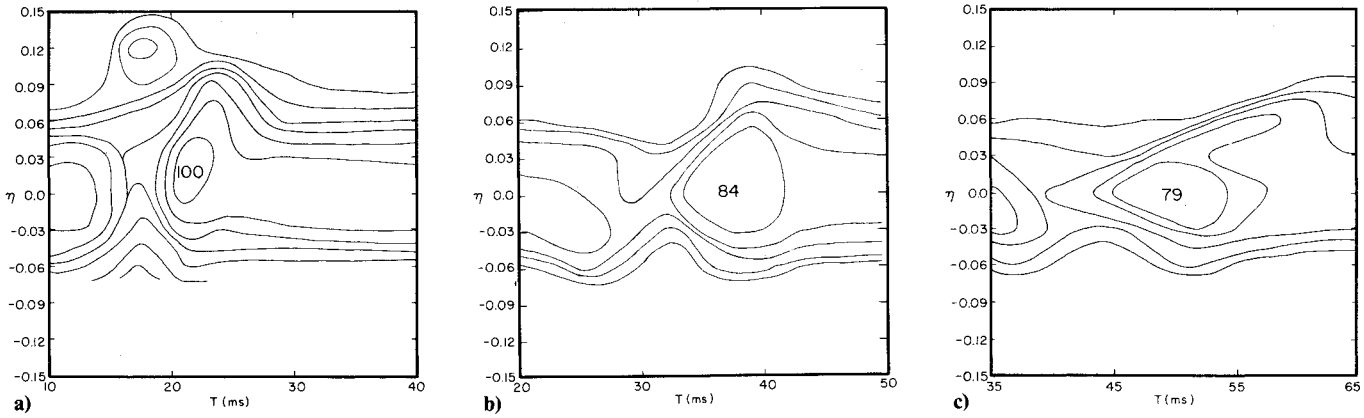

Fig. 16 Contours of phase-averaged intermittency γ_p for $\alpha = 0$ deg. a) $x/D = 1.5$, b) $x/D = 3.0$, c) $x/D = 4.5$.

The distributions of coherent vorticity $\zeta_p = \partial v_p/\partial x - \partial u_p/\partial r$ in the $\alpha = 0$ deg plane for the three stations $x/D = 1.5$, 3.0, and 4.5 are shown in Figs. 15a-c, respectively. For brevity, contours in other α planes are not shown. Note the rather drastic change in the contour from $x/D = 1.5$ to 3.0, while the change between $x/D = 3.0$ and 4.5 is less significant. It is impressive that the alignment and phase averaging has sifted out the underlying coherent structure vorticity. Note that the locations of centers of the vorticity contours do not closely agree with those of the $\langle\psi\rangle$ contours, a result consistent with the single-spark spot data. The vorticity contour peaks occur about 2 ms earlier than the $\langle\psi\rangle$ contour centers. At $x/D = 1.5$, the vorticity contours for the one- and two-spark cases look identical except that the peak vorticity for the two sparks is much higher. The contours for the one-spark case at $x/D = 3.0$ and 4.5 are different from those at the same stations for two sparks. The values of the peak vorticity at $x/D = 1.5$, 3.0, and 4.5 are 1.42, 1.40, and 1.28 times the local maximum time-mean vorticities. The corresponding values for the single-spark spot are 1.08, 1.15, and 1.30. The reason for this difference is not clear.

The contours of coherent structure intermittency are shown in Figs. 16a-c for the stations $x/D = 1.5$, 3.0, and 4.5, respectively, for $\alpha = 0$ deg only. The intermittency signal $I(t)$ was derived on the basis of a threshold determined by the $\partial v/\partial t + A\partial^2 v/\partial t^2$ signal, bandpassed between 300 and 3000 Hz; the parameter A was adjusted such that the ratio of rms values of the two derivatives was unity. Thus, $I(t)$ is biased toward the higher frequency content of the signal. In this sense, the phase-averaged intermittency γ_p is essentially independent of the u_p, v_p, $\langle\psi\rangle$, $(uv)_c$, and ζ_p contours which are determined by the large-scale structures, i.e., at low frequencies. The low value of intermittency γ_p outside the spot is probably due to the fact that irrotational fluid is

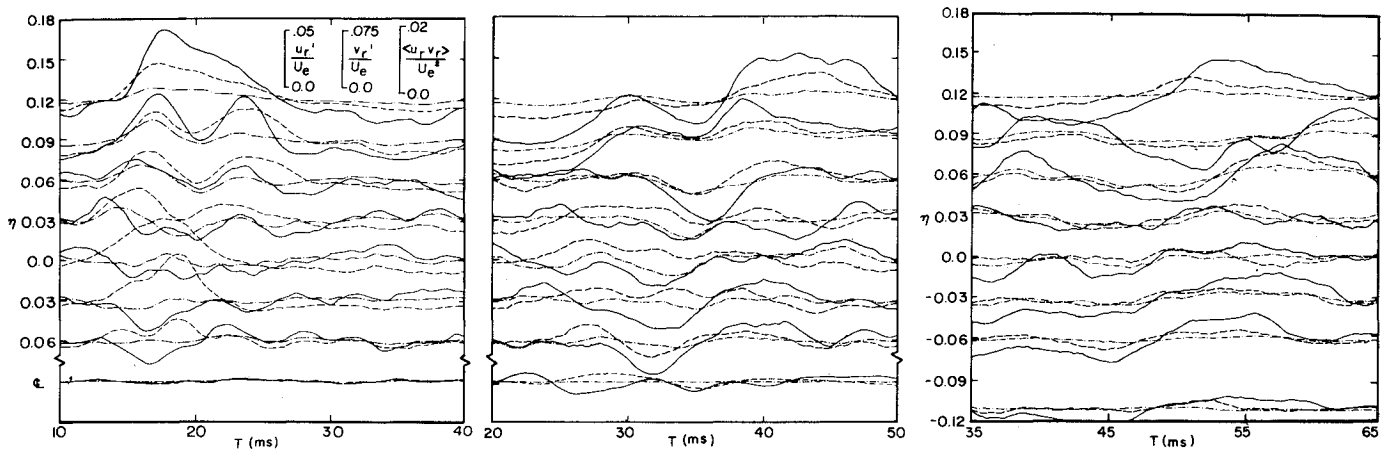

$\hat{u}_r'/U_e$	$\hat{v}_r'/U_e$	$\widehat{u_r v_r}/U_e^2$	$\hat{u}_r'/U_e$	$\hat{v}_r'/U_e$	$u_r v_r/U_e^2$	$\hat{u}_r'/U_e$	$\hat{v}_r'/U_e$	$u_r v_r/U_e^2$
0.087	0.053	0.0019	0.088	0.057	0.0020	0.066	0.036	0.0009
0.118	0.081	0.0041	0.113	0.079	0.0042	0.106	0.066	0.0029
0.138	0.104	0.0060	0.133	0.100	0.0056	0.128	0.092	0.0053
0.155	0.125	0.0082	0.150	0.125	0.0077	0.144	0.111	0.0070
0.154	0.134	0.0085	0.147	0.130	0.0074	0.147	0.12	0.0075
0.133	0.126	0.0077	0.130	0.117	0.0064	0.123	0.100	0.0049
0.095	0.098	0.0042	0.091	0.084	0.0029	0.081	0.073	0.0019
0.037	0.035	0.0012	0.028	0.022	0.0	0.061	0.064	0.0011
a) $x/D=1.5$			b) $x/D=3.0$			c) $x/D=4.5$.		

Fig. 17 Traces of u_r', v_r', $\langle u_r v_r \rangle$ as deviations from corresponding zone averages $\hat{u}_r', \hat{v}_r', u_r v_r$ indicated on the right-hand side; —— u_r', ---- v_r', —·—·— $\langle u_r v_r \rangle$ for $\alpha=0$ deg.

brought from the jet center at the front and from outside (ambient) at the back. This, in combination with the random occurrence of the natural structures, produces the γ_p contours indicating distinct boundaries of the spot. Note that the locations of peak intermittency coincide with the centers of $\langle\psi\rangle$ contours. Thus, even though the spot may be buried in the naturally occurring structures, alignment of the traces with respect to the structure centers accentuates the spot boundary and thus the intermittency. The phase-averaged intermittency drops outside the spot because of the random occurrence of the naturally occurring structures. Note that like the $\langle\psi\rangle$ contours, intermittency contours also suggest that, while the spot grows in size with x, it does not grow as fast as the time-mean width of the mixing layer. Comparison of the single- and two-spark data for $\alpha=0$ deg shows that contours of v_p, $(uv)_c$, and ζ_p are qualitatively similar even though rather different in details.

Figures 17a-c show the time traces of the phase averages of u_r', v_r', and $\langle u_r v_r \rangle$ as functions of η for $x/D=1.5$, 3.0, and 4.5, respectively. For brevity only data in the $\alpha=0$ deg plane are shown. These traces denote the deviations from the respective zone averages, that is the averages over the trace lengths. The corresponding zone average values $\hat{u}_r'$, $\hat{v}_r'$, and $\widehat{u_r v_r}$ are indicated beneath the traces.

In phase-averaged measurements of these kinds, a question naturally arises as to how much of the measured turbulence intensity is due to phase jitter, i.e., numerical turbulence. If the phase jitter effect were dominant, intensities of phase-random fluctuations such as u_r' and v_r' would be large in regions of large gradients of u_p and v_p. Careful comparisons of Figs. 17a-c with Figs. 5-7 and 8-10 show that this is not the case (see also Ref. 10). Thus, it is reasonable to infer that the contributions of phase jitter to quantities such as u_r', v_r', and $\langle u_r v_r \rangle$ are not predominant. It should be emphasized that alignment through time shift is a method of minimizing the effects of phase jitter.

From the spatial distributions of (u_p, v_p), the coherent structure streamlines can be drawn by the method of isoclines.[10,16] It was shown in Ref. 10 that the streamlines agree with the pseudo-streamfunctions in the overall features rather than in details. Thus, the educed coherent structure streamlines are not shown.

Coherent Structure Dynamics

In order to gain some insight into the coherent structure dynamics, contours of phase-averaged properties, namely, $\tilde{u}_p$, $\tilde{v}_p$, $(uv)_c$, ζ_p, γ_p, and $\langle\psi\rangle$, have been educed. The question naturally arises as to which contour provides a clear indication of the boundary of the structure and thus reveals evolution of the structure. Since γ_p contours are based on $I(t)$ signals, these should identify the location of the spot and its average boundary. It is clear that unlike the boundary-layer spot case,[15,16] $\tilde{u}_p$ contours cannot be used to mark the contour of the mixing-layer spot (compare Fig. 5a with Fig. 16a). Similarly, v_p or $\tilde{v}_p$ contours are also not indicative of the spot boundary. It is interesting to note that the phase-averaged vorticity contours also do not agree with the spot center. The locations of peak vorticity or peak $(uv)_c$ typically occur slightly farther downstream (i.e, lower T) than the spot center inferred from the γ_p contours. Only the centers of the $\langle\psi\rangle$ contours agree reasonably well with the centers of the γ_p contours. Thus, the $\langle\psi\rangle$ contours are quite helpful in inferring the overall dynamics and convection characteristics of the spot.

Note that in spite of noticeable differences between the contours of $\tilde{u}_p$, $\tilde{v}_p$, $u_p v_p$, ζ_p, etc., with α at each x, there is good agreement on the location (i.e., T value) of the spot center. The centers of the $\langle\psi\rangle$ contours at $x/D=1.5$ are located at $T=21.6$, 20.7, and 20.3 ms at $\alpha=0$, 45, and 90 deg, respectively. The corresponding centers of $\langle\psi\rangle$ contours are located at 36.8, 35.3, and 36.8 ms for $x/D=3.0$ and at 48.8, 48.6, and 49 ms for $x/D=4.5$. Note that the locations of the peaks of the $(uv)_c$ contours also occur at essentially the same T at each x. Thus, the spot structure at each x is essentially axisymmetric, except that the strength falls off somewhat with increasing α. The variations of the phase-averaged distributions of $\tilde{u}_p$, $\tilde{v}_p$, $u_p v_p$, ζ_p, $\langle\psi\rangle$, u_r', v_r', and $\langle u_r v_r \rangle$ with azimuthal position α should not be taken too seriously, since the observed variations are unavoidable due to the limited positions at which data were taken as well as the limited size of the realizations used in this extremely time-consuming analysis.

Consider the $\alpha=0$ deg plane only. The maximum amplitude of the spot-induced coherent velocities $\tilde{u}_p/U_e$ is 0.29, 0.22, and 0.15 at $x/D=1.5$, 3.0, and 4.5, respectively (see Figs. 5a,

6a, and 7a). The maximum values of $\tilde{v}_p/U_e$ at these stations are 0.1, 0.08, and 0.06, respectively (see Figs. 8a, 9a, and 10a). The peak coherent vorticity values at these stations are 1.42, 1.40, and 1.28 times the corresponding peak time-mean vorticities, respectively. The peaks of the Reynolds stress $u_p v_p/U_e^2$ at the three stations are 0.11, 0.08, and 0.045. The peak values of $(uv)_c/U_e^2$ at these stations are about 0.027, 0.024, and 0.019. These clearly indicate a progressive weakening of the coherent structure with increasing x, as to be expected. For comparison, the maximum time-averaged Reynolds stress is about 0.0085 U_e^2. Thus, even though the coherent Reynolds stress is progressively diluted with increasing x, it is still considerably larger than the background turbulence Reynolds stress.

By identifying the same features in the signals at $x/D=1.5$, 3.0, and 4.5 (i.e., stations 1, 2, and 3), it is possible to deduce the profile of the convection velocity between stations 1 and 2 and between stations 2 and 3. This was done in Ref. 9, but it was shown in Ref. 10 that it is more useful to deduce an overall average convection velocity. Through comparison of the contours of spatial distributions of different coherent structure properties, it was shown in Ref. 10 that $\langle\psi\rangle$ contours give the best estimate of the structure convection velocity. From the peaks of $\langle\psi\rangle$ contours at $x/D=1.5$, 3.0, and 4.5, the convection velocity is found to be 0.60 between stations 1 and 2 and 0.69 between stations 2 and 3. Thus, the use of 0.66 U_e as the reference frame convection velocity in computing $\langle\psi\rangle$ contours was reasonable.

The explanation for the jump in the average convection velocity between the two spatial regions in x is not clear. The corresponding increase in the convection velocity for the single spark was lower. This could be due to acceleration of the spot in x. Another possibility is that the structure undergoes pairing with natural structures, presumably between stations 1 and 2. The abrupt change in the contours between stations 1 and 2 is not inconsistent with such a conjecture. In order to answer this question, it is necessary to obtain these measurements at closer x stations and, further, to obtain spatial distributions of the properties without involving the Taylor hypothesis. However, this would require a prohibitively large amount of computer time.

It should be mentioned that the zone averages $\hat{u}_r'$ and $\hat{v}_r'$ of the phase-averaged background turbulence intensities u_r' and v_r' over the trace length, i.e., over the physical extent of the spot, are essentially the same as the corresponding time-mean values. One can thus infer that the induced structure, whose aspect ratio also agrees with that of the naturally-occurring structure,[5,17] is probably a natural structure triggered by the two sparks.

Conclusion

In an attempt to understand the evolution and dynamics of the coherent structures in the nearfield of a circular jet, the spot structure induced by two sparks fired simultaneously at diametrically opposite points near the lip of a circular air jet was investigated. The spark-induced structure, buried in the large-amplitude fluctuations in the axisymmetric mixing layer, has been educed.

From the phase-averaged time traces of x-wire outputs, spatial distributions of the coherent longitudinal and lateral motions, Reynolds stress, vorticity, streamlines, and intermittency have been derived. It is shown that the phase averages of background turbulence intensities and Reynolds stress do not contain large contributions due to phase jitter. Thus, the eduction scheme has been successful in sifting out the spot signature.

From azimuthal distribution of the educed contours of flow variables, it is clear that the induced structure is essentially an axisymmetric structure, which undergoes complicated interactions, presumably through tearing as well as pairing with the natural structures as it travels downstream.[8] These interactions as well as the evolution of azimuthal structures[14] produce so many changes that there appears to be no similarity between the structures at the three stations studied. It also appears that the spot is a naturally occurring large-scale coherent structure triggered by the two sparks.

The fact that the two-spark-induced structure is essentially axisymmetric and is somewhat similar to the one generated by a single spark in an azimuthal plane passing through the spark center and the jet axis, tends to suggest that the transition is probably triggered downstream in the mixing layer by the acoustic disturbance induced by the sparks. In spite of progressive weakening with x, the coherent Reynolds stress at the end of the potential core, i.e., at $x/D=4.5$, is considerably larger than the background turbulence Reynolds stress. The fact that the spot generated by the two sparks is almost axisymmetric and similar to the single-spark-induced spot, suggests that it is a representative of the typical natural structures in the axisymmetric layer. The detailed dynamics of the mixing layer is the result of interactions of these "spots."

Acknowledgment

This research was supported by the National Science Foundation under Grant ENG-7822110 and the Office of Naval Research under Grant N00014-76-0128.

References

[1] Brown, G. L. and Roshko, A., "On Density Effects and Large Structures in Turbulent Mixing Layers," *Journal of Fluid Mechanics*, Vol. 64, 1976, pp. 775-816.

[2] Winant, C. D. and Browand, F. K., "Vortex Pairing: The Mechanism of Turbulent Mixing Layer Growth at Moderate Reynolds Number," *Journal of Fluid Mechanics*, Vol. 63, 1974, pp. 237-255.

[3] Crow, S. C. and Champagne, F. H., "Orderly Structure in Jet Turbulence," *Journal of Fluid Mechanics*, Vol. 48, 1971, pp. 547-591.

[4] Bruun, H. H., "A Time-Domain Analysis of the Large-Scale Flow Structure in a Circular Jet, Part 1: Moderate Reynolds Number," *Journal of Fluid Mechanics*, Vol. 83, 1977, pp. 641-671.

[5] Yule, A. J., "Large Scale Structure in the Mixing Layer of a Round Jet," *Journal of Fluid Mechanics*, Vol. 89, 1978, pp. 413-432.

[6] Lau, J. C. and Fisher, M. J., "The Vortex-Street Structure of 'Turbulent Jets,' Part 1," *Journal of Fluid Mechanics*, Vol. 67, 1975, pp. 299-337.

[7] Lau, J. C., "The Vortex-Structure of Turbulent Jets, Part 2," submitted to *Journal of Fluid Mechanics*.

[8] Hussain, A.K.M.F. and Clark, A. R., "On the Coherent Structure of the Axisymmetric Mixing Layer: A Flow-visualization Study," *Journal of Fluid Mechanics*, Vol. 104, 1981, pp. 263-294.

[9] Sokolov, M., Hussain, A.K.M.F., Kleis, S. J., and Husain, Z. D., "A 'Turbulent Spot' in an Axisymmetric Free Shear Layer, Part 1," *Journal of Fluid Mechanics*, Vol. 98, 1980, pp. 65-95.

[10] Hussain, A.K.M.F., Kleis, S. J., and Sokolov, M., "A 'Turbulent Spot' in an Axisymmetric Free Shear Layer, Part 2," *Journal of Fluid Mechanics*, Vol. 98, 1980, pp. 97-135.

[11] Husain, Z. D. and Hussain, A.K.M.F., "Axisymmetric Mixing Layer: Influence of the Initial and Boundary Conditions," *AIAA Journal*, Vol. 17, 1979, pp. 48-55.

[12] Kleis, S. J., "The Effect of Exit Conditions on the Development of an Axisymmetric Turbulent Free Jet," Ph.D. Dissertation, Michigan State University, East Lansing, 1974.

[13] Hussian, A.K.M.F. and Reynolds, W. C., "The Mechanics of an Organized Wave in Turbulent Shear Flow," *Journal of Fluid Mechanics*, Vol. 41, 1970, pp. 241-258.

[14] Hussain, A.K.M.F. and Zaman, K.B.M.Q., "Vortex Pairing in a Circular Jet Under Controlled Excitation, Part 2, Coherent Structure Dynamics," *Journal of Fluid Mechanics*, Vol. 101, 1980, pp. 493-544.

[15] Zilberman, M., Wygnanski, I., and Kaplan, R. E., "Transitional Boundary Layer Spot in a Fully Turbulent Environment," *The Physics of Fluids*, Vol. 20, 1977, pp. S258-S271.

[16] Cantwell, B. J., Coles, D., and Dimotakis, P., "Structure and Entrainment in the Plane of Symmetry of a Turbulent Spot," *Journal of Fluid Mechanics*, Vol. 87, 1978, pp. 641-672.

[17] Hussain, A.K.M.F. and Zaman, K.B.M.Q., "The 'Preferred Mode' of the Axisymmetric Jet," *Journal of Fluid Mechanics*, 1981, (to be published).